ELSEVIER

Chemical Engineering Journal 87 (2002) 31–40

Chemical Engineering Journal

www.elsevier.com/locate/cej

Enhanced CO_2 diffusion in wedges

M.E. Aguilera [a], R.L. Cerro [b], A.L. López de Ramos [a,*]

[a] *Grupo de Investigación Fenómenos de Transporte (GFT), Departamento de Termodinámica y Fenómenos de Transferencia, Universidad Simón Bolívar, Apartado Postal 89000, Caracas 1080A, Venezuela*

[b] *Department of Chemicals and Materials Engineering, College of Engineering, University of Alabama, Huntsville, AL, USA*

Received 10 December 1999; received in revised form 27 June 2001; accepted 4 July 2001

Abstract

A porous media is a collection of particles of different shapes and sizes. Particles can be deformed such that they rarely contact at a point, but on extended surfaces. As a consequence of these contacts between particles, the resulting voids can present a large number of cusp-like sections resulting in a low-angle intersection of solid surfaces. Depending on the angle at which surfaces interact and on the contact angle between a liquid and the solid surface, a meniscus will rise on a wedge in a similar way a liquid meniscus rises inside a capillary. If the sum of the half-angle of the wedge and the contact angle is less than $\pi/2$, there is no possible equilibrium shape and a liquid filament will rise to fill the entire length of the wedge. It was found that filaments have an active role in the enhanced diffusion process between carbon dioxide and liquid hydrocarbons. The presence of filament not only increases the mass transfer area but also plays an important role in the convective mixing process that occurs inside the pore.

Keywords: CO_2 diffusion; Diffusion in wedge; Filament rise

1. Introduction

The rate of interfacial mass transfer inside porous rocks is very important to the design and operation of enhanced oil recovery processes. A typical example is carbon dioxide recovery where the mechanism of recovery consists of dissolving CO_2 in hydrocarbons, with the result of the swelling of the liquid phase and migration of the hydrocarbon from the pockets to the open pores. The rate of mass transfer is affected by three principal factors, which are: (1) mass transfer coefficient between phases; (2) interfacial area; (3) departure from equilibrium.

The mass transfer coefficient is a measure of the mass transfer between phases by a combination of convection and diffusion. Ideally, two phases in contact at a flat interface would transfer mass by a diffusion mechanism only. In practice, there are many causes for convective currents that usually enhance the rate of mass transfer between interfaces. Density gradients caused by composition or thermal differences give rise to convective currents and surface tension gradients.

The interfacial area between phases plays a direct, extensive role in mass transfer. Contact between phases is assumed to happen at an idealized Gibb's 2D surface. By modifying the area of this surface, the mass transfer rate can be affected in a quantitative way. Departure from equilibrium is measured through characteristic concentration differences in each phase. The farther from equilibrium the concentration of a component is, the faster the transfer of the component across the interface will be. Understanding the incidence of these factors on mass transfer in a porous network is the key to control the rate of the overall mass transfer process. The principal goal of this work was to understand the enhanced diffusion process that takes place between carbon dioxide and light hydrocarbons and study all the possible interfacial area configurations for a gas that is soluble in a liquid in a 2D, semi-infinite domain.

1.1. Diffusion process

Understanding the fundamentals of the diffusion process in multicomponent systems is an important step to investigate convective mass transfer effects due to capillary forces, since these effects can easily mask each other. Little detailed work has been done regarding the effect of capillary forces on convective mixing inside pores. Preliminary evidence indicates that CO_2 absorption affects the wetting behavior of the liquid hydrocarbons and can lead to capillary-generated flows (via surface energy gradients) in interstitial spaces with narrow angles of contact.

* Corresponding author. Present address: PAKMAIL PD 1010, P.O. Box No. 02 5304, Miami, FL 33102-5304, USA. Tel.: +1-582-906-3743; fax: +1-582-906-4113.
E-mail address: alopez@usb.ve (A.L. López de Ramos).

1385-8947/02/$ – see front matter
PII: S1385-8947(01)00209-1

Nomenclature

a	diameter of capillaries [L]
A_L, A_V	constants in Eqs. (11) and (12)
D	mutual diffusion coefficient [$L^2\,T^{-1}$]
h	meniscus height [L]
J	mass flux of a component [$M\,L^{-2}\,T^{-1}$]
L	liquid bridge length, bubble length [L]
L_0	liquid bridge initial length [L]
L^*	equivalent displacement [L]
m	slope of line describing interface growth [$L\,T^{-1/2}$]
M	molecular weight [$M\,N^{-1}$]
R_c	radius of curvature of the corner of the square capillary [L]
R_t	radius of curvature of the filament at the top [L]
R_0	radius of curvature of the liquid meniscus [L]
t	time [T]
T	temperature [Q]
v	specific volume of a component [$L^3\,M^{-1}$]
V	phase average velocity [L T]
w	mass fraction of a component [–]
x	position in a phase [L]
X	position of an interface [L]
ΔZ_{total}	total filament elevation [L]

Greek letters

α	geometrical interior angle [–]
δ	filament thickness at the top [L]
θ	contact angle [–]
κ	capillary constant [L^{-2}]
μ	viscosity [$M\,L^{-1}\,T^{-2}$]
ρ	density [$M\,L^3$]
σ	surface tension [$M\,T^2$]

Subscripts

b	bubble in experiment
f	interface
i, j	components in a phase
L	liquid component if it is placed at the begin and liquid phase if it is alone or at the end
V	vapor component if it is placed at the begin and vapor phase if it is alone or at the end

Superscripts

m	velocity or mass flux relative to local mass-average velocity
V	velocity or mass flux relative to local volume-average velocity
*	concentration in a saturated phase

In this case, the modeling of boundary effects is very important.

Diffusion coefficients of CO_2 reported by different authors in the literature differ from each other by about an order of magnitude. Convective effects have been blamed for these discrepancies found in experimental values of diffusion coefficients [7]. Measurements by Renner [11] showed that different values of diffusion coefficients could be obtained in Berea sandstone depending on the vertical or horizontal position of the rock. Convective effects justified most of these discrepancies. Reporting flow visualization displacement by CO_2 in model pores, Campbell and Orr [4] commented on the differences between displacement of Soltrol and oil and pointed out the importance of wetting behavior and the geometry of the pores. They were the first ones to mention the paper by Concus and Finn [6] and the presence of what are called capillary-active surfaces.

1.2. Capillary-active surfaces

The name capillary-active surfaces is used here to denote capillary surfaces that, because of their particular geometry, can experience large changes in configuration or promote convective patterns when undergoing a heat and/or mass transfer process. The basis for this definition is a very important concept related to equilibrium configurations, developed by Concus and Finn [6] during the analysis of the capillary rise of the equilibrium-free surface of a liquid when the liquid partially fills a container with a corner. The cross-section of the container, otherwise circular, encloses a corner with an interior angle equal to 2α. Concus and Finn found that the shape of the free surface at the corner changes dramatically depending on the value of $\alpha+\theta$, where θ is the contact angle at the three-phase contact line. When $\alpha+\theta < \pi/2$, the surface does not have a finite equilibrium position and the capillary surface raises unbounded, i.e. never reaching an equilibrium configuration.

A porous media is a collection of particles of different shapes and sizes. Particles can be deformed such that they rarely contact at a point, but on extended surfaces. As a consequence of these contacts between particles, the resulting voids can present a large number of cusp-like sections resulting in the low-angle intersection of solid surfaces. Depending on the angle at which surfaces interact and on the contact angle between a liquid and the solid surface, liquid filaments can rise filling the entire length of the wedge.

Early works on fluid dynamics in porous media modeled the porous voids as a network of circular capillaries. In recent years, the need for angularity in the capillary paths has been recognized and models of meniscus displacement as well as bubble breakup and coalescence have been developed with the use of square capillaries. A geometry that can be used to simulate porous media is given by a capillary of square cross-section (Fig. 1). The reason for investigating the mass transfer process that occurs in capillaries of square cross-section is because the pore shapes in oil reservoirs

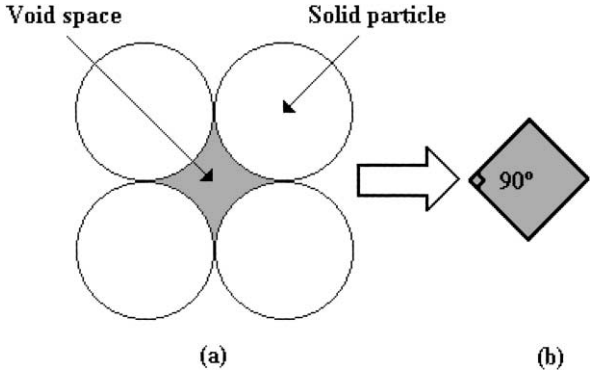

Fig. 1. Geometry used to simulate porous media: (a) real model; (b) ideal model.

are more like rectangular shapes than circular ones [3]. The role of capillary-active surfaces becomes important when the interfacial properties of the liquid phase as well as the contact angle of the three-phase system are changing in time and space due to mass transfer. A typical situation arises in enhanced oil recovery when the absorption of CO_2 in liquid hydrocarbon alters the interfacial tension of the liquid–gas interface as well as the contact angle. Changes in contact angle result in changes of the equilibrium shape of the liquid in contact with these capillary active surfaces.

2. Diffusion experiments

Substantial differences can be found for mass transfer rates in CO_2–hydrocarbon systems, depending on the type of capillary used, circular or square. The set of possible geometries for the interaction of a gas and a liquid inside capillaries are shown in Fig. 2 [2,8]. The contact of two unbounded phases is shown in Fig. 2a. This experiment will be denoted as the 'liquid pool experiment'. A finite liquid phase immersed in an unbounded gas phase will be denoted as the 'liquid bridge experiment' (Fig. 2b). The 'shrinking bubble experiment', shown in Fig. 2c, is an example of a finite gas phase immersed in an unbounded liquid phase. These three geometries span the set of possible problems for a gas that is soluble in the liquid in a 2D, semi-infinite domain.

2.1. Liquid pool

The liquid pool experiments are simple and easy to perform [1,8]. The capillaries used were 1 mm × 1 mm square tubing (Wilmad, catalog number WST-8100), 2 mm × 2 mm square tubing (Wilmad, catalog number WS-102) and 2 mm circular capillary (Wilmad, precision bore capillary tubing, ID = 0.8 and 1.9913 mm). The hydrocarbons chosen for the liquid phase were *n*-decane (Aldrich Chemical, 99+%) and 2,2,4-trimethylpentane (Aldrich Chemical, 99+%). The gas phase used was carbon dioxide (Coleman, 99.99%). Fig. 3 shows the details of the viewing cell and auxiliaries. Certain

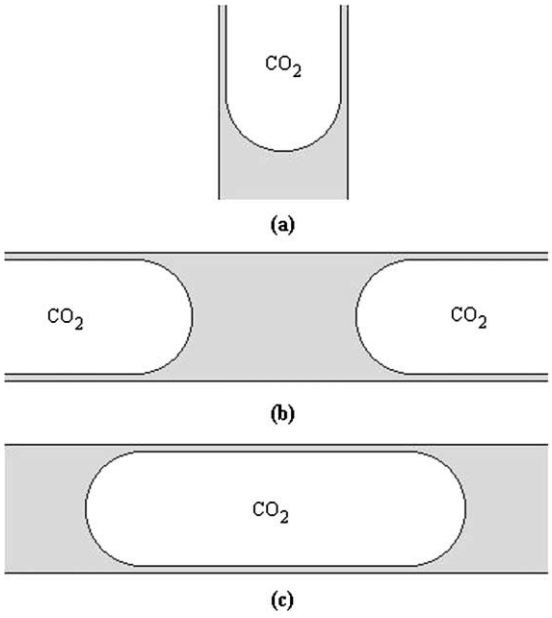

Fig. 2. The three different geometries for the mass transfer experiments: (a) liquid pool; (b) liquid bridge; (c) shrinking bubble.

amount of liquid is placed in the liquid reservoir (C_n). The liquid reservoir vessel, with all its connections, is evacuated using a vacuum pump (Welch, Duo Seal, model number 1400) for 10 min. The rest of the viewing cell and fitting is evacuated. When the evacuation process is completed, liquid is introduced from the bottom of the capillary. Carbon dioxide is injected to the top of the capillary at pressures between 1000 and 2300 kPa.

The pool of liquid, from a theoretical point of view, can be considered to be semi-infinite, i.e. a reasonable boundary condition to apply will be that the concentration of CO_2 in the hydrocarbon goes to zero as the depth of the liquid pool goes to negative infinity. In the experiments, the liquid pool is infinite and it is confined in a space of constant

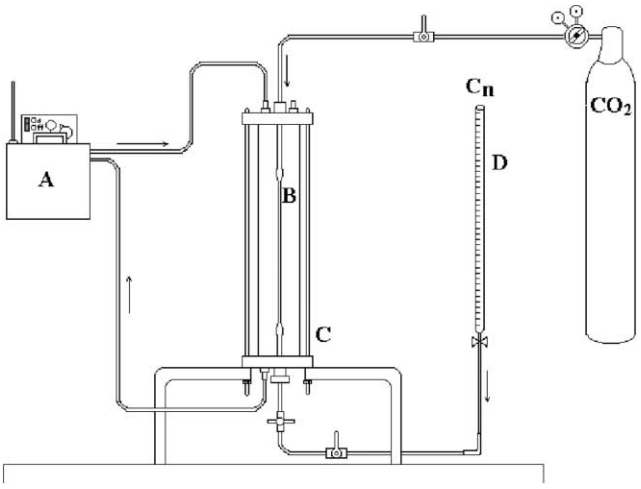

Fig. 3. Details of viewing cell and auxiliaries. A: glycerol; B: capillary; C: cell of Plexiglas; D: hydrocarbon.

volume. As a result of mass transfer of carbon dioxide into the liquid hydrocarbon, the volume of the liquid changes and this change in volume can be measured as the displacement of the gas–liquid interface.

A video-camera system was placed in front of the cell focusing the interface between the gas and the liquid phase, lighted from behind using a flexible fiber optic system. The change in meniscus height was followed using a linear translator with a micrometer. The experiment was recorded using a video-system. Image processing was done using the Targa-Truvision system. Variation of the meniscus height with time was computed. In all cases, the meniscus displacements were larger in the square capillary than in the circular one. If the interfaces were flat (90° contact angle) for the same displacement, the equivalent volume for the square capillary would be bigger than the circular one. The meniscus shapes are far from being flat for all the hydrocarbon–CO_2 systems studied. In fact, in the cases of *n*-decane and 2,2,4-trimethylpentane, the filaments are formed in the square capillary increasing the total mass transfer area. In order to compare the two experiments using the same basis, an empirical value called equivalent displacement, L^*, was defined using the following relationship:

$$L^* = \frac{\text{Volume displaced}}{\text{Mass transfer area}} \tag{1}$$

With the technique suggested by López de Ramos and Cerro [9], and assuming that the filament shapes do not change with time, Eq. (1) can be written as follows:

For the circular capillary:

$$L^* = \frac{a^2 z(t)}{2R_0 h} \tag{2}$$

For the square capillary:

$$L^* = \frac{2a^2 z(t)}{\pi R_0 h + (R_t + (1/(h\kappa + (2/R_b))))((\pi/2) - 2\theta)\Delta Z_{total}} \tag{3}$$

The variables a, R_0 and h are defined in Fig. 4. R_t is the filament radius of curvature at the top, θ the contact angle

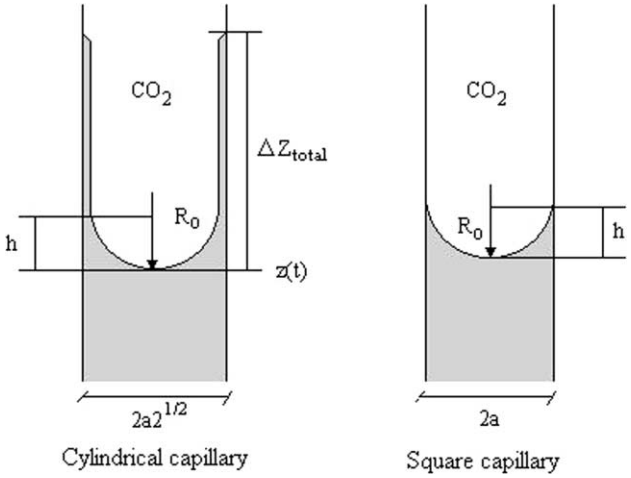

Fig. 4. Geometrical definition of the variables used for the calculation of L^* [12].

in radians, R_b the radius of curvature of the liquid meniscus, ΔZ_{total} the filament elevation and κ the capillary constant defined as $\kappa = \rho g/\sigma$.

All the filament geometrical values and the contact angles are shown in Appendix A. These values were taken from López de Ramos and Cerro [9] who developed a method assuming a spherical-segment meniscus. The total elevation ΔZ_{total} of the filament with respect to the liquid level in the capillary is given as a function of κ, R_t and R_b

$$\Delta Z_{total} = \frac{1}{\kappa}\left[\frac{1}{R_t} - \frac{2}{R_b}\right] \tag{4}$$

López de Ramos and Cerro [9] also related the contact angle at the gas–liquid–solid contact line with the radius of the rounded corner of capillary, R_c, and the radius of curvature of the liquid filament, R_t in the following equation:

$$\tan\theta = \frac{R_c - \sqrt{2R_t^2 - R_c^2}}{\sqrt{2}\sqrt{R_t^2 + R_c\sqrt{2R_t^2 - R_c^2}}} \tag{5}$$

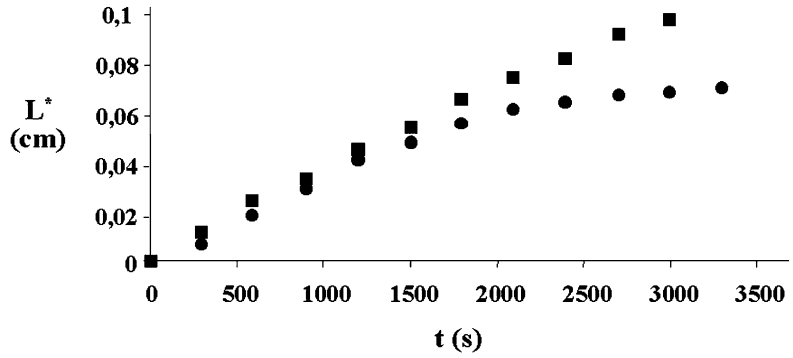

Fig. 5. Equivalent displacement of the interface for 2,2,4-trimethylpentane–carbon dioxide at $P = 1400$ kPa. (■) 2 mm square capillary; (●) 2 mm cylindrical capillary.

Eq. (5) can be used to compute the contact angle if ΔZ_{total}, R_t and R_c are known.

Fig. 5 shows the values of L^* as a function of $t^{1/2}$. Notice that in all the cases, the square capillary response is above the circular capillary curve.

When hydrocarbons are pressurized with carbon dioxide, a relative strong activity is detected in the liquid, especially near the interface. This activity can be described as "threads" [5] of dense solution (the density of CO_2–hydrocarbon solution is bigger than the pure hydrocarbon) falling down through the liquid. These phenomena can be easily observed due to the difference in refractive indexes between the CO_2–hydrocarbon solution and the pure hydrocarbon. It is evident that convection patterns are present in the liquid phase. Experiments done with 2,2,4-trimethylpentane and CO_2 at a pressure of 2000 kPa show a deformed meniscus and small wave-like patterns along the surface. The interfacial activity observed at the square capillary was more intense than the one observed at the circular capillary.

2.2. Liquid bridge

The experimental set-up using in the liquid bridge experiments is similar to the one shown in Fig. 3, but the capillary was placed in horizontal position. Using a syringe and a long needle (10 cm) with a very small diameter (less than 0.5 mm), the liquid hydrocarbon was introduced near the center of the capillary. It is important to avoid touching the walls of the capillary with the needle to prevent pre-wetting. In horizontal square capillaries, the liquid filaments have a constant cross-section that spans the length of the capillary. Additional quantities of liquid need to be introduced to create a liquid bridge of a given length in order to fill the corners of the square tubing. The final form of the liquid bridge is shown in Fig. 6a. In the case of the circular capillary, no film was detected and the liquid bridge shape is sketched in Fig. 6b. Once the liquid was inside the capillary,

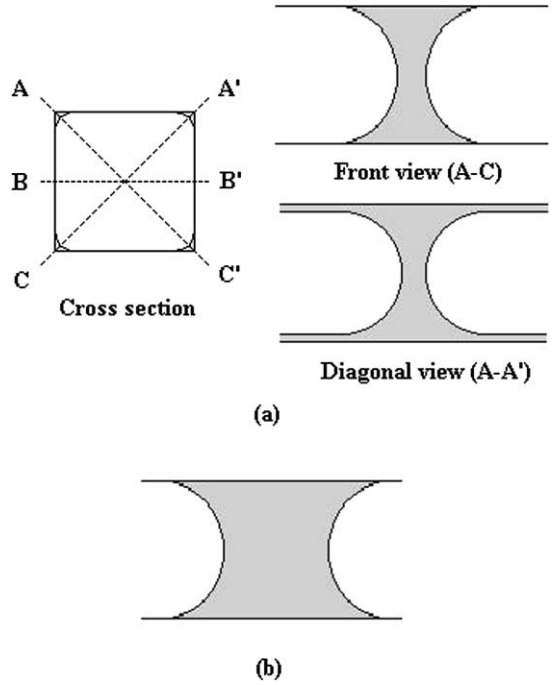

Fig. 6. Liquid bridges in square (a) and cylindrical capillaries (b).

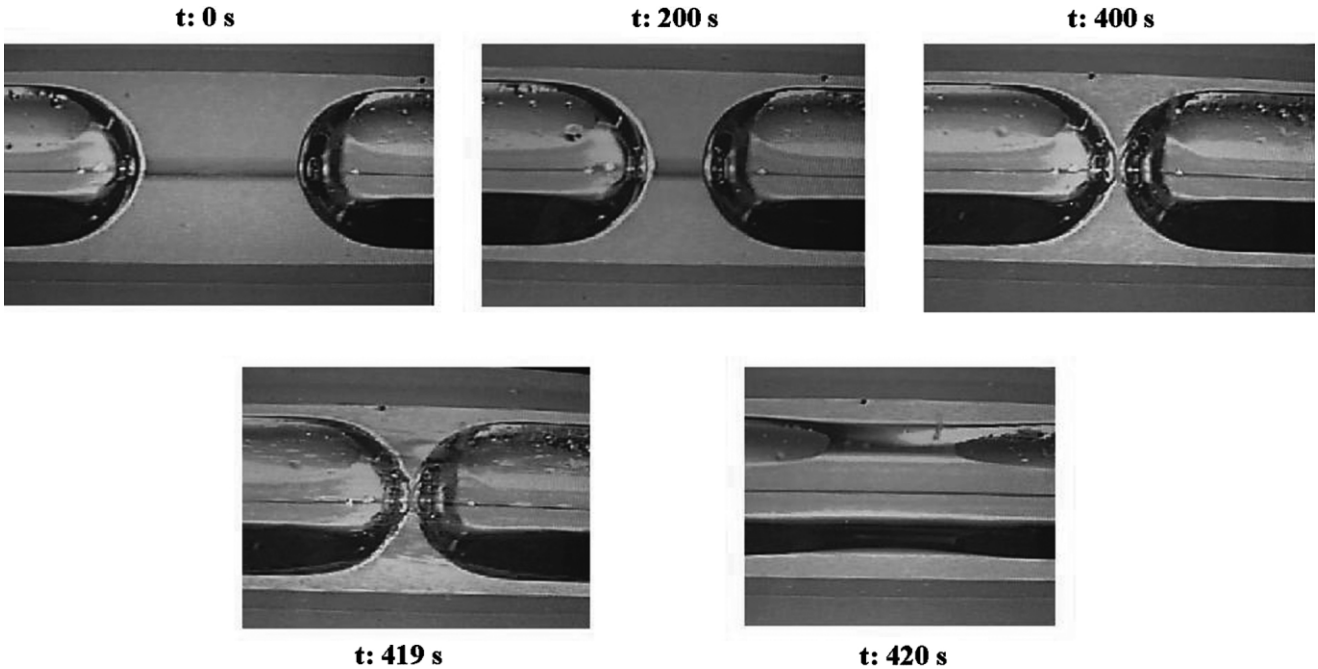

Fig. 7. Sequence of photographs showing the reducing process of the length of the bridge (square capillary).

CO_2 was injected from both sides of it up to a pressure of 1000 kPa.

The behavior of the square capillary liquid bridge was totally different from the behavior in the circular capillary. In the square capillary, the length of the liquid bridge decreases with the time up to the point that the two interfaces touch and the liquid bridge breaks up.

Fig. 7 shows a sequence of illustrations showing the length reducing process. This reduction process is relatively fast, and certainly faster than evaporation or interfacial mass transfer. Fig. 8 shows that in circular capillary, the length of the liquid bridge increases with time. The increment in length was slow because mass transfer was very slow, but it showed a totally different behavior than the square capillary. The total change of the bridge was around 2 mm in a period of time of almost 6 h, which is compatible with the rate of volume increase of the hydrocarbon due to solution of CO_2.

Fig. 9 shows the change in length of the liquid bridges for square and circular capillaries as a function of time. It is evident that the liquid hydrocarbon is being pumped through the filaments up to the ends of the square capillary. This process cannot occur in the circular capillary because there is not a continuos liquid film to promote the movement of the liquid phase.

An additional experiment was performed in the square capillary with *n*-decane and air, with no mass transfer taking place between the gas and the liquid phase. At the beginning, the liquid bridge stood firmly in place and no change in volume was detected. After 3 h, however, the length of the liquid bridge decreased and it shrunk until the bridge disappeared at a rate similar to the experiments done in the presence of carbon dioxide. It is obvious that in the absence of CO_2, the contact angle was large enough for the hysteresis of the contact angle to prevent the movement of the filaments. Perturbations or the creeping of the precursor film may have caused the movement to start and when it was started it went to the end of the capillary, as it was expected. This phenomenon has an enormous implication on the recovery rate of isolated lumps of oil trapped inside a continuos pore open at both ends.

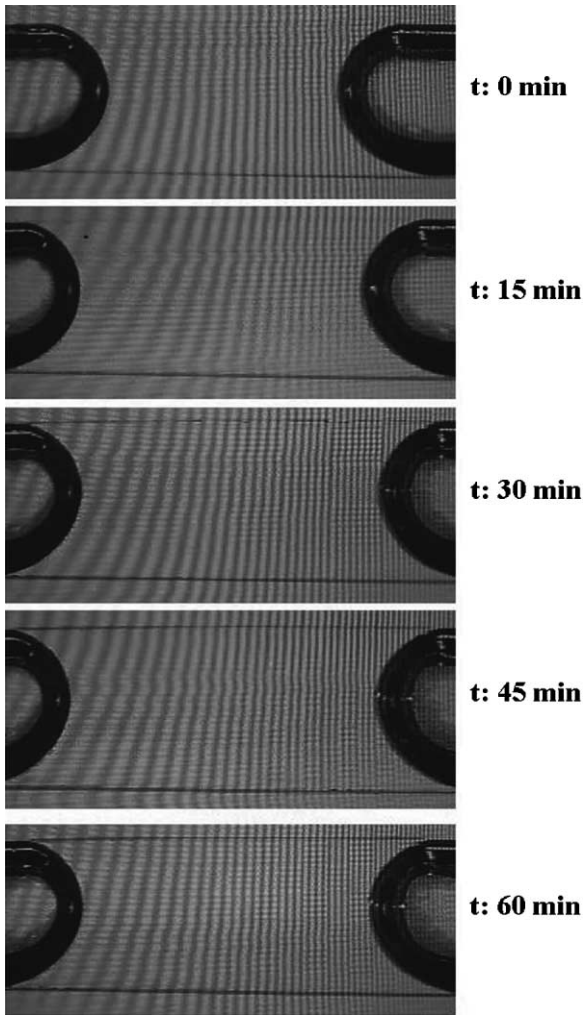

Fig. 8. Sequence of photographs showing the increasing process of the length of the bridge (circular capillary).

Knowing the geometry of the system and the variation of the thickness of the bridge, it is possible to estimate the velocity at what the liquid is pumped through the filaments. The velocity values are between 0.1 and 2 cm/s.

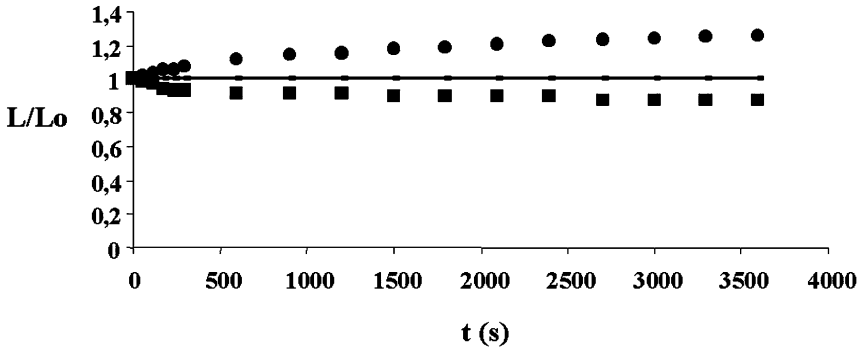

Fig. 9. Liquid bridge length as a function of time for decyl alcohol–carbon dioxide at $P = 600$ kPa (■) 2 mm square capillary; (●) 2 mm cylindrical capillary.

2.3. Shrinking bubble

The shrinking experimental technique was used to measure diffusion of CO_2 in hydrocarbons. Experiments were performed at 25 °C and 2300 kPa. The hydrocarbon used was *n*-decane (99+% from Aldrich Chemical) and the vapor phase was carbon dioxide (Coleman Grade, 99.99%). Fig. 10 shows the set-up used to create a vapor bubble surrounded by the liquid phase. A video-camera system was used to record the changes in length of the bubble as a function of time. Different capillaries were used with the purpose of evaluating the effect of size and shape of capillaries in this type of measurements.

2.3.1. Mathematical model

Considering the motion of the interface relative to a fixed frame of reference as well as relative to the local vapor and liquid phase volume and mass-average velocities, the relationship between these velocities may be written [7]:

$$\frac{\mathrm{d}X_{\mathrm{L}}}{\mathrm{d}t} = \frac{\partial X_{\mathrm{L}}^{\mathrm{V}}}{\partial t} + V_{\mathrm{L}}^{\mathrm{V}}(X_{\mathrm{L}}) = \frac{\mathrm{d}X_{\mathrm{V}}^{\mathrm{V}}}{\mathrm{d}t} + V_{\mathrm{V}}^{\mathrm{V}}(X_{\mathrm{L}}) \tag{6}$$

$$\frac{\mathrm{d}X_{\mathrm{L}}}{\mathrm{d}t} = \frac{\partial X_{\mathrm{L}}^{\mathrm{m}}}{\partial t} + V_{\mathrm{L}}^{\mathrm{m}}(X_{\mathrm{L}}) = \frac{\mathrm{d}X_{\mathrm{V}}^{\mathrm{m}}}{\mathrm{d}t} + V_{\mathrm{V}}^{\mathrm{m}}(X_{\mathrm{L}}) \tag{7}$$

Eqs. (6) and (7) state that for each phase, the velocity of the interface relative to a fixed reference frame is equal to the sum of the velocity of the interface relative to the phase volume or mass-average velocity and that velocity, which is always measured relative to the fixed reference frame.

For a binary system $w_{\mathrm{V,L}} = 1 - w_{\mathrm{V,V}}$.

$$\frac{\mathrm{d}X_{\mathrm{L}}^{\mathrm{V}}}{\mathrm{d}t} = \frac{D_{\mathrm{L}}((\partial w_{\mathrm{V,L}}/\partial x) - D_{\mathrm{V}})(\rho_{\mathrm{V}}/\rho_{\mathrm{L}})(\partial w_{\mathrm{V,V}}/\partial x)}{w_{\mathrm{V,V}}^{*} - w_{\mathrm{V,L}}^{*}} \tag{8}$$

The transient diffusion equations for the vapor component in the liquid and vapor phases written for coordinate systems moving with the phase mass-average velocity are

$$\rho_{\mathrm{L}}\frac{\partial w_{\mathrm{V,L}}}{\partial t} = \rho_{\mathrm{L}} D_{\mathrm{L}}\frac{\partial^2 w_{\mathrm{V,L}}}{\partial x_{\mathrm{L}}^2} \tag{9}$$

and

$$\rho_{\mathrm{V}}\frac{\partial w_{\mathrm{V,V}}}{\partial t} = \rho_{\mathrm{V}} D_{\mathrm{V}}\frac{\partial^2 w_{\mathrm{V,V}}}{\partial x_{\mathrm{V}}^2} \tag{10}$$

where x_{L} and x_{V} are coordinates moving with the liquid and vapor mass-average velocities, respectively. With the additional assumption that the liquid and vapor phases are semi-infinite in extent, Eqs. (9) and (10) have analytical solutions:

$$w_{\mathrm{V,L}}^{*} = w_{\mathrm{V,L}}(x_{\mathrm{L}}, 0) + A_{\mathrm{L}}\left[1 + \mathrm{erf}\left(\frac{X_{\mathrm{L}}^{\mathrm{V}}}{2\sqrt{D_{\mathrm{L}}t}}\right)\right] \tag{11}$$

$$w_{\mathrm{V,V}}^{*} = w_{\mathrm{V,V}}(x_{\mathrm{V}}, 0) + A_{\mathrm{V}}\left[1 - \mathrm{erf}\left(\frac{X_{\mathrm{V}}^{\mathrm{V}}}{2\sqrt{D_{\mathrm{V}}t}}\right)\right] \tag{12}$$

where A_{L} and A_{V} are constants.

To be admissible solutions to the problem Eqs. (11) and (12) must satisfy the conditions

$$X_{\mathrm{L}}^{\mathrm{V}} = 2\lambda\sqrt{D_{\mathrm{L}}t} \tag{13}$$

$$X_{\mathrm{V}}^{\mathrm{V}} = 2\lambda\beta\sqrt{D_{\mathrm{V}}t} \tag{14}$$

where λ and β are constants of the system and can be evaluated as follows:

$$\beta = \frac{\rho_{\mathrm{L}}}{\rho_{\mathrm{V}}}\sqrt{\frac{D_{\mathrm{L}}}{D_{\mathrm{V}}}} \tag{15}$$

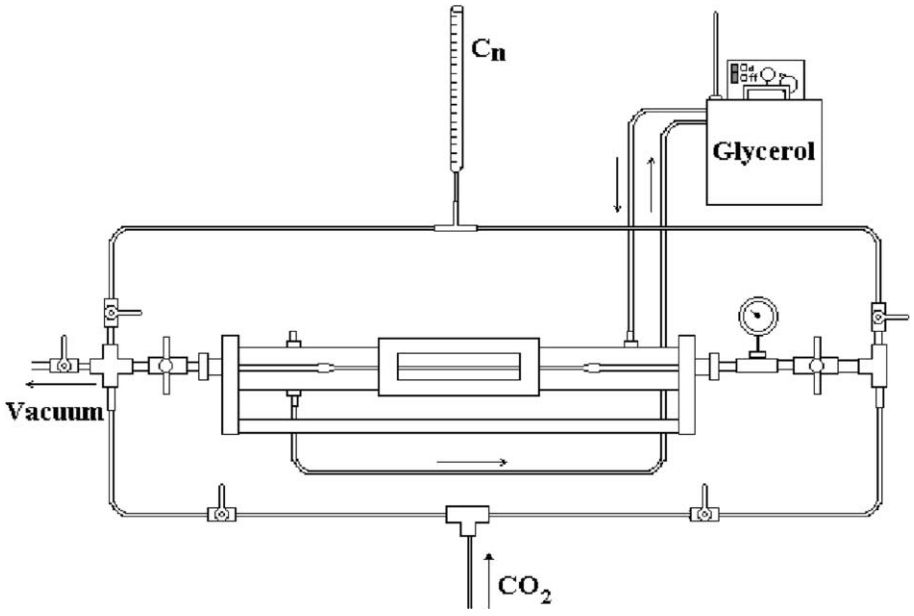

Fig. 10. Arrangement of a diffusion cell experiment: shrinking bubble.

$$\lambda = \frac{1}{\sqrt{\pi}(w^*_{V,V} - w^*_{V,L})} \left\{ \frac{[w^*_{V,L} - w_{V,L}(x_L, 0)]\exp(-\lambda^2)}{1 + \mathrm{erf}(\lambda)} - \frac{1}{\beta} \frac{[w_{V,V}(x_V, 0) - w^*_{V,V}]\exp(-\lambda^2\beta^2)}{1 - \mathrm{erf}(\lambda\beta)} \right\} \quad (16)$$

For large values of β, the second term of Eq. (16) can be neglected.

An expression for X^V_V could be

$$X^V_V(t) = \tfrac{1}{2}[X_b(0) - X_b(t)] \quad (17)$$

where $X_b(0)$ is the initial length of the CO_2 bubble and $X_b(t)$ is the subsequent lengths recorded during the diffusion experiment.

Combination of Eqs. (13)–(15) and (17) yields the relationship between the growth of the interface relative to the liquid phase and the experimentally observed shrinkage of the vapor phase.

$$X^V_L(t) = \frac{1}{2}\frac{\rho_V}{\rho_L}[X_b(0) - X_b(t)] \quad (18)$$

Substitution of Eq. (13) into (18) gives:

$$X_b(t) = X_b(0) - m\sqrt{t} \quad (19)$$

where

$$m = 4\lambda\sqrt{D_L}\frac{\rho_L}{\rho_V} \quad (20)$$

The procedure for calculating the diffusivity of CO_2 in the hydrocarbon is to plot the observed bubble length against $t^{1/2}$. This should result in a linear plot of slope $-m$. Eq. (20) is then used to calculate D_L. Measurement of phase composition is not required and the equilibrium data was taken from [10].

2.3.2. Experimental results

Fig. 11 shows experimental data obtained for the 2 mm square capillary. The sequence of photographs shows the reducing process of the CO_2 bubble in a square capillary.

Fig. 12 shows bubble length as a function of $t^{1/2}$ for *n*-decane–carbon dioxide system at 38 °C. Two capillaries were used, the 0.8 mm cylindrical and the 2 mm square. In the case of cylindrical capillary, the experimental data can be fitted well by a straight line when the bubble length is plotted against the square root of time; this behavior points out that there is no evidence of convective diffusion in cylindrical capillaries of small diameters (<1 mm). This result agrees with the values reported by Grogan et al. [7], López de Ramos [8], and Aguilera [1]. In the square capillary experiment, the experimental values deviate from the straight line predicted by theory, although they were performed at lower pressure (500 kPa). This deviation can be attributed not only to convective mixing (as it was reported by Grogan et al. [7]), but to the presence of filaments. Filaments increase the mass transfer area and promote the movement of the liquid from one bubble side to the other. Therefore, if square capillaries are used, an effective diffusion coefficient will be obtained.

The diffusion coefficient calculated using experimental data from cylindrical capillary is shown in Fig. 13. Contrary as it would be expected from theory, the diffusivity coefficient of liquid is a function of pressure (as pressure increases, diffusivity decreases). This result can be easily

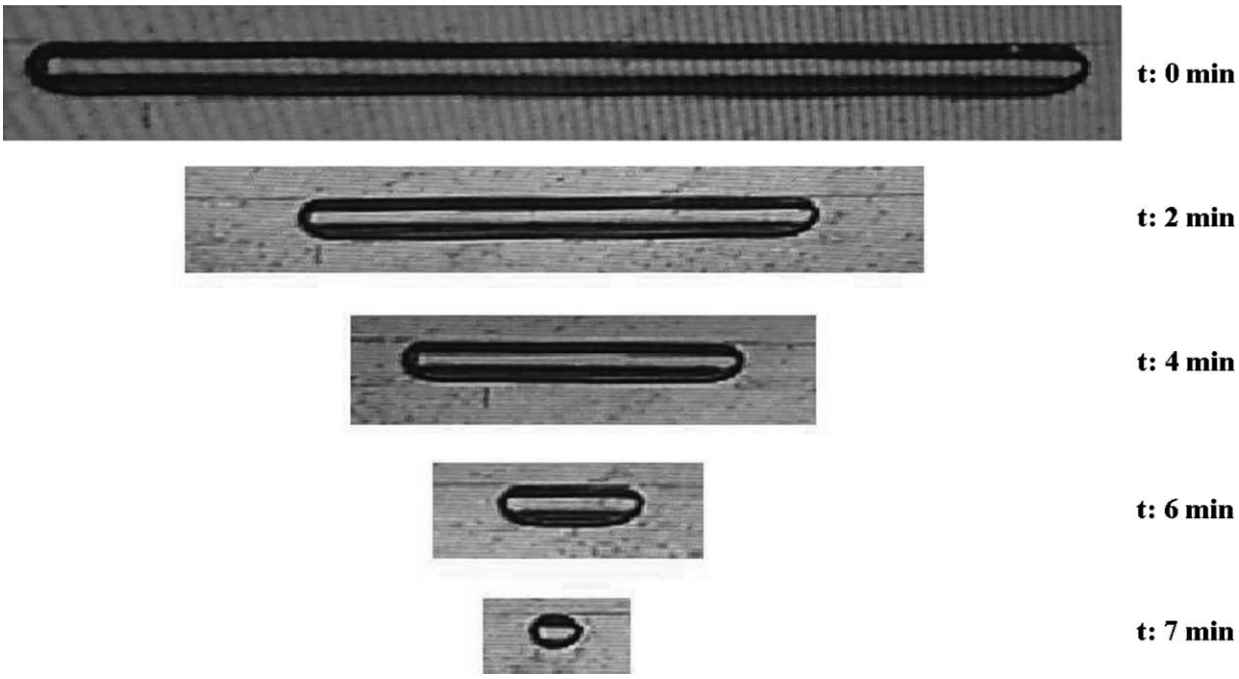

Fig. 11. Sequence of photograph showing the reducing process of the length of the bubble for *n*-decane–carbon dioxide at $P = 1500$ kPa and 38 °C.

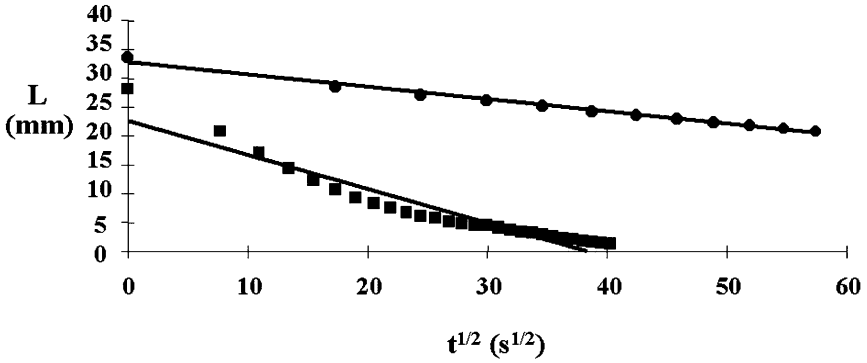

Fig. 12. Bubble length as a function of time for *n*-decane–carbon dioxide system. (■) 2 mm square capillary at $P = 500$ kPa, $T = 38°C$; (●) 0.8 mm cylindrical capillary at $P = 2600$ kPa, $T = 38°C$.

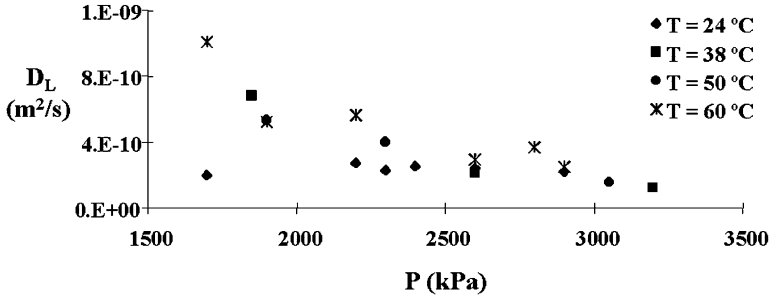

Fig. 13. Diffusion coefficient of liquid phase at different temperatures and pressures for *n*-decane–carbon dioxide system (0.8 mm cylindrical capillary).

explained by the swelling process that the gas–liquid mixture suffers, since the liquid phase does not behave as an incompressible fluid. The effect of temperature is less evident, although there is a clear tendency for the diffusivity coefficient to increase as temperature increases.

Fig. 14 shows diffusion coefficient as a function of pressure at different temperatures. A behavior similar to the one observed in cylindrical capillary was found. Nevertheless, diffusion coefficients of almost two orders of magnitude larger than the ones computed using the 0.8 mm cylindrical capillary were obtained. It seems that diffusivity and pressure are related by a lineal function in square capillaries, while in cylindrical tubing, this relationship becomes exponential. With the use of square capillaries, a different shape of the gas–liquid interface is introduced. For square capillaries, the capillary surface at the corners spans the length of the bubble. This shape of interface develops because the contact angle (θ) for decane is very small (10.3°) and the geometrical angle (2α) is 90°. As a consequence, $\alpha + \theta < \pi/2$. The resulting capillary surface creates a convective mixing pattern different, and obviously more active, than the circular capillary (2 mm diameter). These capillary-active surfaces lead to an enhancement of diffusion process because of the interface increases and convective diffusion appears. In modeling of crude oil recovery from reservoirs, wedges are not considered and recovery

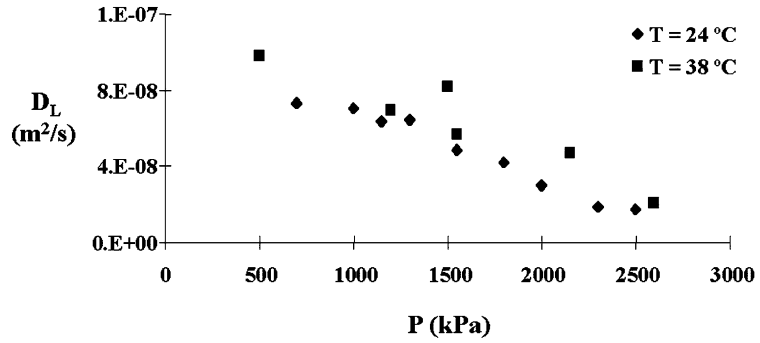

Fig. 14. Diffusion coefficient of liquid phase at different temperatures and pressures for *n*-decane–carbon dioxide system (2 mm square capillary).

yields are until 40% more than the calculated values in models.

3. Summary and concluding remarks

This research work helped to understand the role of interfacial phenomena in mass transfer between a gas, such as CO_2, and a liquid hydrocarbon in wedges. When a hydrocarbon absorbs CO_2, the interfacial tension between the gas and the liquid phase, as well as the contact angle at the three-phase (solid–gas–liquid) contact line, are affected. Increasing the concentration of CO_2 decreases the interfacial tension and the contact angle.

A combination of three different experiments (liquid pool, liquid bridge and shrinking bubble) represented the possible arrays for a gas that is soluble in a liquid in a 2D, semi-infinite domain. Substantial differences were found for mass transfer rates in CO_2–hydrocarbon systems, depending on the cross-section (cylindrical or square) of the capillary used.

In shrinking bubble experiments inside cylindrical capillaries, the experimental data can be fitted well by a straight line when the bubble length is plotted against the square root of time. At the same experimental condition, the behavior of the gas–liquid system deviated from the straight line predicted by theory when the experiments took place inside square capillary tubes. This deviation can be attributed to convective mixing. This convection movement was originated by the gradient of density as well by the presence of the liquid filaments at the corners.

The diffusion coefficients calculated using the experimental data from square capillaries is an order of magnitude larger than the one computed using a cylindrical tubes. With the use of square capillaries, the capillary surface at the corners spans the length of the bubble. This shape of interface develops because the contact angles for decane and 2,2,4-trimethylpentane are very small (10.3 and 7.3°, respectively) and the geometrical angle (2α) is 90°. As a consequence, $\alpha + \theta < \pi/2$. The resulting capillary surface creates a convective mixing pattern different, and obviously more active, than the circular capillary.

The filaments present at the four corners of the square capillary play an active role in the enhanced diffusion process between carbon dioxide and liquid hydrocarbons. The presence of filaments not only increases the mass transfer area, but also plays an important role in the convective mixing process that occurs inside the pore.

Acknowledgements

Financial support by Decanato de Investigaciones, Sección de Fenómenos de Transporte of the Universidad Simon Bolivar and CONICT Project 95-000476 is gratefully acknowledged by authors.

Appendix A

Radii of curvature and contact angle values for the 2 mm square capillary, taken from [9]

Liquid	Radii of curvature (m)				
	ΔZ_{total} (m) (experimental)	R_b ($\times 10^6$) (experimental)	R_c ($\times 10^6$) (experimental)	R_t ($\times 10^6$) (experimental)	θ (°) (calculated)
n-Decane	0.01852	1136	103	128	10.3 ± 0.3
2,2,4-Trimethylpentane	0.01745	1108	103	119	7.3 ± 0.3

References

[1] M.E. Aguilera, Estudio de la transferencia de masa en regiones capilares, M.Sc. Dissertation, Universidad Simón Bolívar, 1999.
[2] M.E. Aguilera, A.L. López de Ramos, Mass transfer in capillary regions, in: Proceedings of the 13th International Congress of Chemical and Process Engineering (CHISA 98), Lecture D6.8, Summaries 4.
[3] K. Birdi, D. Vu, A. Winter, A. Norregard, Capillary rise of liquids in rectangular tubings, Colloid Polym. Sci. 266 (5) (1988) 470–474.
[4] B. Campbell, F. Orr, Flow visualization for CO_2/crude oil displacements, Soc. Petrol. Eng. J. (1995) 665–678.
[5] F.O. Chukwuma, Mass transfer of gaseous carbon dioxide into a quiescent liquid hydrocarbon, Doctor of Philosophy Dissertation, The University of Tulsa, 1983.
[6] P. Concus, R. Finn, On the behavior of a capillary-free surface in a wedge, Proc. Natl. Acad. Sci. USA 63 (1969) 292–299.
[7] A. Grogan, V. Pinczewski, G. Russkauff, F. Orr, Diffusion of CO_2 at reservoir conditions: Models and Measurements, SPE Reservoir Eng. (1988) 93–102.
[8] A.L. López de Ramos, Capillary enhanced diffusion of CO_2 in porous media, Doctor of Philosophy Dissertation, The University of Tulsa, 1993.
[9] A.L. López de Ramos, R.L. Cerro, Liquid filament rise in corners of square capillaries: a novel method for the measurement of small contact angles, Chem. Eng. Sci. 49 (14) (1994) 2395–2398.
[10] H. Reamer, B. Sage, Phase equilibria in hydrocarbon systems. Volumetric and phase behavior of the *n*-decane–CO_2 system, J. Chem. Eng. Data 8 (4) (1963) 508–513.
[11] T. Renner, Measurement and correlation of diffusion coefficient for CO_2 and rich gas applications, SPE 15391 (1986) 1–12.
[12] G. Washburn, The dynamics of capillary flow, Phys. Rev. 17 (1921) 273–283.